



A decoupled energy stable scheme for a hydrodynamic phase-field model of mixtures of nematic liquid crystals and viscous fluids



Jia Zhao^a, Xiaofeng Yang^a, Jie Shen^b, Qi Wang^{c,a,d,*}

^a Department of Mathematics, University of South Carolina, Columbia, SC 29208, United States

^b Department of Mathematics, Purdue University, West Lafayette, IN 47907, United States

^c Beijing Computational Science Research Center, Beijing, 100094, China

^d School of Mathematics, Nankai University, Tianjin, 300071, China

ARTICLE INFO

Article history:

Received 20 May 2015

Received in revised form 9 August 2015

Accepted 24 September 2015

Available online 21 October 2015

Keywords:

Phase field

Energy stable scheme

Liquid crystals

Free surface flows

Finite difference

GPU

ABSTRACT

We develop a linear, first-order, decoupled, energy-stable scheme for a binary hydrodynamic phase field model of mixtures of nematic liquid crystals and viscous fluids that satisfies an energy dissipation law. We show that the semi-discrete scheme in time satisfies an analogous, semi-discrete energy-dissipation law for any time-step and is therefore unconditionally stable. We then discretize the spatial operators in the scheme by a finite-difference method and implement the fully discrete scheme in a simplified version using CUDA on GPUs in 3 dimensions in space and time. Two numerical examples for rupture of nematic liquid crystal filaments immersed in a viscous fluid matrix are given, illustrating the effectiveness of this new scheme in resolving complex interfacial phenomena in free surface flows of nematic liquid crystals.

© 2015 Elsevier Inc. All rights reserved.

1. Introduction

The binary phase field model, also known as the diffuse interface model, is a tool to resolve the motion of free interfaces between two distinct fluid components, whose origin can be traced back to Rayleigh [23] and Van der Waals [30]. It was first formulated to study material mixtures and later adopted as a technique to resolve motion of the interface between different material components in material mixtures [2,4,37]. With the new development in advanced algorithms and computational technologies recently, it has emerged as an efficient method to resolve complex dynamics in interfacial fluid flows involving complex topological changes. An advantage of the phase-field approach is that the model is often derived from a variational principle with an energy dissipation law, making it possible to carry out rigorous mathematical analyses, including the existence and uniqueness of the solution of the governing partial differential equations. It also makes it plausible to design the numerical scheme that obeys an analogous discrete energy dissipation law, warranting nonlinear stability in the numerical computation [3,11,12,22,28,29,34]. For more details about the numerical methods developed for phase field models, readers are referred to some recent review papers [15,25] and the references therein.

* Corresponding author at: Beijing Computational Science Research Center, Beijing, 100094, China; Department of Mathematics, University of South Carolina, Columbia, SC 29208, United States.

E-mail addresses: zhaog2@math.sc.edu (J. Zhao), xfyang@math.sc.edu (X. Yang), shen@math.purdue.edu (J. Shen), qwang@math.sc.edu (Q. Wang).

Recently, Shen and Yang [27] developed a new numerical scheme for solving a hydrodynamic phase-field model for binary mixture flows of liquid crystals and viscous fluids, where the phase field transport equation is the Allen–Cahn equation [27]. Since the commonly used Allen–Cahn equation does not conserve the fluid volume, they used the Lagrangian multiplier method to enforce the volume conservation in their scheme. They proved that the new scheme satisfies a semi-discrete energy law, leading to decoupled, elliptic equations to be solved at each time step, and is unconditionally stable in time. The type of schemes that obeys an analogous, discrete energy dissipation law is customarily called the energy stable scheme. In order to prove the energy stability for the scheme, however, they did not use the time invariant derivative in the director transport equation and in the meantime omitted the corresponding elastic stress for the liquid crystal component in the model as well. The mathematical convenience leads to a model that no longer describes the liquid crystal component well in flows of the fluid mixture, i.e., the model is no longer frame indifference.

In this paper, we extend the previous study to a hydrodynamic phase field model for the binary mixture flow of liquid crystals and viscous fluids, in which the Cahn–Hilliard equation is adopted as the transport equation for the phase variable so that the volume of the mixture fluid is automatically conserved. We devise a new semi-discrete scheme in time and then prove the scheme is energy stable for the full model without any modification. This is by no means an easy task due to highly nonlinear couplings among the velocity, the hydrostatic pressure, the phase field function (or variable), the director field for liquid crystals, the time invariant derivative and the nontrivial elastic stress tensor. We note that this approach also applies to the Allen–Cahn model with the correct invariant time derivative for the director vector and elastic stress, extending the work of [27]. In addition, the anchoring energy, where the liquid crystal has preferred orientation at the interface, has also been considered. Specifically, we design an energy stable numerical scheme in a semi-discrete form in time and show that it satisfies the following properties: (a) it is unconditionally stable in time; (b) it satisfies a discrete energy law; and (c) it leads to decoupled, elliptic equations to be solved at each time step so that fast solvers for elliptic equations can be employed. We then implement this numerical scheme on graphic processing units (GPUs) using CUDA to conduct the mesh refinement test and to study rupture dynamics of a nematic liquid crystal drop or a filament immersed in a viscous fluid matrix [32]. Numerical experiments demonstrate the desired accuracy in the mesh refinement test in time and the presented numerical examples capture some interesting phenomena when the liquid crystal filament ruptures.

The rest of the paper is organized as follows. In Section 2, we describe a hydrodynamic phase-field model for the mixture flow of nematic liquid crystals and viscous fluids using the Cahn–Hilliard equation as the phase transport equation and derive the associated energy dissipation law. In Section 3, we develop the decoupled, energy stable numerical scheme for the coupled nonlinear hydrodynamic equation system. In Section 4, we prove the semi-discrete energy law for the new numerical scheme. In Section 5, we present the mesh refinement test results and a couple of numerical examples to illustrate the efficiency of the proposed scheme and study dynamics of nematic liquid crystal drops and filaments immersed in a viscous fluid matrix.

2. Two-phase hydrodynamic model for mixtures of nematic liquid crystals and viscous fluids

We consider a two-phase hydrodynamic phase field model for immiscible mixtures of nematic liquid crystals (LC) and viscous fluids. The volume fraction of the liquid crystal phase is represented by a phase function ϕ ,

$$\phi(x, t) = \begin{cases} 1 & \text{liquid crystal,} \\ 0 & \text{viscous fluid,} \end{cases} \quad (2.1)$$

with a thin smooth transitional layer of thickness ε separating the liquid crystal phase from the viscous fluid phase. The interface of the mixture is described by the level set $\Gamma_t = \{x : \phi(x, t) = \frac{1}{2}\}$. Without loss of generality, we assume all model parameters are already non-dimensionalized and therefore dimensionless.

The total energy of the mixture fluid system \mathcal{E} is given by

$$\mathcal{E} = \int_{\Omega} \left[\frac{1}{2} \rho |\mathbf{u}|^2 dx + F \right] dx, \quad (2.2)$$

where the first part is the kinetic energy E_{kin} with ρ the volume averaged density of the mixture and \mathbf{u} the volume-averaged fluid velocity and the second part is the material system's free energy. The free energy contains three parts: the mixing free energy E_b , the bulk free energy for liquid crystals E_d , and the anchoring energy for liquid crystals E_{anch} [34],

$$F = E_b + E_d + E_{anch}. \quad (2.3)$$

Specifically, we denote $f(\phi) = \frac{1}{\varepsilon^2} \phi^2 (1 - \phi)^2$ as the Ginzburg–Landau double-well potential and define the mixing free energy by

$$E_b = \int_{\Omega} \gamma \left(\frac{1}{2} |\nabla \phi|^2 + f(\phi) \right) dx, \quad (2.4)$$

where γ is the strength of the energy proportional to the traditional surface tension [34] and the gradient term measures the conformational entropy.

We assume that the bulk energy for liquid crystals is given by the modified Oseen–Frank distortional energy with a penalizing bulk term for handling potential defects in the liquid crystal phase [8,16,17,20,35]:

$$E_{\mathbf{d}} = \int_{\Omega} \frac{1}{2} \phi^2 W(\mathbf{d}) d\mathbf{x}, \quad W(\mathbf{d}) = K \left(\frac{1}{2} |\nabla \mathbf{d}|^2 + g(\mathbf{d}) \right) \tag{2.5}$$

where K is the Frank elastic constant [6] and $g(\mathbf{d}) = \frac{1}{4\delta^2} (|\mathbf{d}|^2 - 1)^2$ is a Ginzburg–Landau type penalty term, introduced to approximate the unit length constraint of \mathbf{d} [18,19], where δ is a model parameter measuring the size of the defect core.

At the interface between the viscous fluid and the liquid crystal, a surface energy known as the anchoring energy is necessary to yield a preferred orientation for the liquid crystal [6,13]. The anchoring energy is given by

$$E_{anch} = \int_{\Omega} \left[\frac{A_1}{2} (\mathbf{d} \cdot \nabla \phi)^2 + \frac{A_2}{2} (|\mathbf{d}|^2 |\nabla \phi|^2 - (\mathbf{d} \cdot \nabla \phi)^2) \right] d\mathbf{x}, \tag{2.6}$$

where A_1 and A_2 ($A_1 > 0, A_2 > 0$) are the strength for the planar and **homotropic** anchoring energy, respectively.

Assuming (i) the phase field variable obeys the Cahn–Hilliard dynamics, (ii) the nematic director follows a relaxation dynamics in the Allen–Cahn form [2,9,21,22], (iii) the two fluids have a matching constant density $\rho = 1$ and viscosity η , we obtain the following dimensionless governing system of equations:

$$\begin{cases} \partial_t \mathbf{u} + \mathbf{u} \cdot \nabla \mathbf{u} = -\nabla p + \eta \Delta \mathbf{u} + \nabla \cdot \tau_e - \phi \nabla \mu - \mathbf{h} \nabla \mathbf{d}, \\ \nabla \cdot \mathbf{u} = 0, \\ \partial_t \mathbf{d} + \mathbf{u} \cdot \nabla \mathbf{d} - \mathbf{W} \cdot \mathbf{d} = a \mathbf{D} \cdot \mathbf{d} + M_1 \mathbf{h}, \\ \partial_t \phi + \nabla \cdot (\mathbf{u} \phi) = M_2 \Delta \mu, \end{cases} \tag{2.7}$$

where

$$\begin{aligned} \tau_e &= -\frac{a}{2} (\mathbf{d}\mathbf{h} + \mathbf{h}\mathbf{d}) + \frac{1}{2} (\mathbf{d}\mathbf{h} - \mathbf{h}\mathbf{d}), \\ \mu &= \gamma (\Delta \phi - f(\phi)) - K \phi W(\mathbf{d}) - (A_1 - A_2) \nabla \cdot ((\mathbf{d} \cdot \nabla \phi) \mathbf{d}) - A_2 \nabla \cdot (|\mathbf{d}|^2 \nabla \phi), \\ \mathbf{h} &= \nabla \cdot \left(-\frac{K \phi^2}{2} \nabla \mathbf{d} \right) + \frac{K \phi^2}{2} g'(\mathbf{d}) - (A_1 - A_2) (\mathbf{d} \cdot \nabla \phi) \nabla \phi - A_2 |\nabla \phi|^2 \mathbf{d}. \end{aligned} \tag{2.8}$$

Here $\mu = \frac{\delta F}{\delta \phi}$ is the chemical potential [36], $\mathbf{h} = -\frac{\delta F}{\delta \mathbf{d}}$ the molecular field, τ_e is the elastic stress tensor associated with liquid crystal dynamics [33], $\mathbf{D}_{\alpha\beta} = \frac{1}{2} (\partial_\beta \mathbf{u}_\alpha + \partial_\alpha \mathbf{u}_\beta)$ is the rate of strain tensor, $\mathbf{W}_{\alpha\beta} = \frac{1}{2} (\partial_\beta \mathbf{u}_\alpha - \partial_\alpha \mathbf{u}_\beta)$ is the vorticity tensor, p is the hydrostatic pressure, $1/M_1$ is the relaxation time parameter of LC director dynamics, M_2 is the mobility parameter of the phase field function, a is a geometry parameter of liquid crystal molecules and η is the volume averaged viscosity.

Remark 2.1. When the two fluids have different densities with a relatively small difference, one can use the Boussinesq approximation [22]. The case of different viscosities can usually be dealt with in a straightforward manner by assuming the viscosity is a linear or harmonic average of the phase function.

Throughout the paper, we assume the following boundary conditions for the hydrodynamic variables and the internal variables:

$$\mathbf{u}|_{\partial\Omega} = 0, \quad \nabla \phi \cdot \mathbf{n}|_{\partial\Omega} = 0, \quad \nabla \mu \cdot \mathbf{n}|_{\partial\Omega} = 0, \quad \nabla \mathbf{d} \cdot \mathbf{n}|_{\partial\Omega} = 0, \tag{2.9}$$

with \mathbf{n} the unit outward normal, which warrants the boundary effect does not contribute to the energy dissipation. In fact, all results presented in this paper are valid for periodic boundary conditions as well.

Notice the fact that this system is energy dissipative, which enables us to prove the existence and uniqueness of the weak solution with certain smoothness by a standard Galerkin procedure [7]. The time rate of change of the total energy is given by

$$\begin{aligned} \frac{d\mathcal{E}}{dt} &= \int_{\Omega} \mathbf{u} \cdot \partial_t \mathbf{u} + \frac{\delta F}{\delta \phi} \frac{\partial \phi}{\partial t} + \frac{\delta F}{\delta \mathbf{d}} \frac{\partial \mathbf{d}}{\partial t} d\mathbf{x} \\ &= \int_{\Omega} \mathbf{u} \cdot \left(-\mathbf{u} \cdot \nabla \mathbf{u} - \nabla p + \eta \Delta \mathbf{u} - \phi \nabla \mu - \mathbf{h} \nabla \mathbf{d} + \nabla \cdot \left(-\frac{a}{2} (\mathbf{d}\mathbf{h} + \mathbf{h}\mathbf{d}) + \frac{1}{2} (\mathbf{d}\mathbf{h} - \mathbf{h}\mathbf{d}) \right) \right. \\ &\quad \left. + \mu (-\nabla \cdot (\mathbf{u} \phi) + M_2 \Delta \mu) - \mathbf{h} (-\mathbf{u} \cdot \nabla \mathbf{d} + \mathbf{W} \cdot \mathbf{d} + a \mathbf{D} \cdot \mathbf{d} + M_1 \mathbf{h}) \right) d\mathbf{x} \\ &= \int_{\Omega} -\nabla \cdot \left(\mathbf{u} \frac{|\mathbf{u}|^2}{2} \right) + \frac{|\mathbf{u}|^2}{2} \nabla \cdot \mathbf{u} - \nabla \cdot (p \mathbf{u}) + p \nabla \cdot \mathbf{u} - \nabla \cdot (\mu \phi \mathbf{u}) \end{aligned}$$

$$\begin{aligned}
 & + \nabla \cdot \left(-\frac{a}{2}(\mathbf{d}\mathbf{h} + \mathbf{h}\mathbf{d})\mathbf{u} + \frac{1}{2}(\mathbf{d}\mathbf{h} - \mathbf{h}\mathbf{d})\mathbf{u} \right) + \nabla \cdot (\eta\mathbf{u}\nabla\mathbf{u}) - \eta|\nabla\mathbf{u}|^2 \\
 & - M_1|\mathbf{h}|^2 + \nabla \cdot (M_2\mu\nabla\mu) - M_2|\nabla\mu|^2 d\mathbf{x} \\
 = & - \int_{\Omega} (\eta|\nabla\mathbf{u}|^2 + M_1|\mathbf{h}|^2 + M_2|\nabla\mu|^2) d\mathbf{x}.
 \end{aligned} \tag{2.10}$$

Clearly, the parameters η , M_1 and M_2 affect the magnitude of the dissipation rate.

3. Decoupled semi-discrete scheme

One of the desirable properties for the discretized dissipative system to have is to maintain its own energy dissipation law that is consistent with the energy law obeyed by the continuous differential system. Practically, this is an indication for a good approximation to the differential dissipative system. In the following, we will design a semi-discrete energy stable scheme that addresses the following issues:

- the coupling of the velocity and pressure through the incompressible condition;
- the stiffness in the phase field equation and the director equation associated with the interfacial width ε and the defect core size δ ;
- nonlinear couplings among the momentum transport equation, the phase transport equation and the director equation.

In doing so, we develop the scheme based on a stabilization technique [26]. To prove energy stability of the scheme, we have to put some constraints on the potential function $f(\phi)$ and $g(\mathbf{d})$, i.e., they satisfy the following conditions: (i) f and g have continuous second order derivatives, (ii) there exist constants L_1 and L_2 such that

$$\max_{|\mathbf{d}| \in \mathbb{R}^3} |\mathbf{H}(\mathbf{d})| \leq L_2, \quad \max_{|\phi| \in \mathbb{R}} |f''(\phi)| \leq L_1, \tag{3.1}$$

where $\mathbf{H}(\mathbf{d})$ is the Hessian matrix of $g(\mathbf{d})$.

One immediately notice that this condition is not satisfied by the double-well potentials $f(\phi) = \frac{1}{\varepsilon^2}\phi^2(\phi - 1)^2$ and $g(\mathbf{d}) = \frac{1}{4\delta^2}(|\mathbf{d}|^2 - 1)^2$. However, we can modify $f(\phi)$ to the quadratic growth outside of a physically meaningful interval $[-M, M]$ without affecting the solution if the maximum norm of the initial condition ϕ_0 is bounded by M . Analogously, we can modify the function g outside a ball in \mathbb{R}^3 of radius M . For instance, we propose the following modifications:

$$\tilde{f}(\phi) = \begin{cases} \frac{1}{\varepsilon^2}\phi^2, & \phi < 0, \\ \frac{1}{\varepsilon^2}\phi^2(1 - \phi)^2, & 0 \leq \phi \leq 1, \\ \frac{1}{\varepsilon^2}(1 - \phi)^2, & \phi > 1, \end{cases} \quad \tilde{g}(\mathbf{d}) = \begin{cases} \frac{1}{4\delta^2}(1 - |\mathbf{d}|^2)^2, & |\mathbf{d}| \leq 1, \\ \frac{1}{\delta^2}(1 - |\mathbf{d}|)^2, & |\mathbf{d}| > 1. \end{cases} \tag{3.2}$$

Therefore, it is common (cf. [5,14,26]) to consider the Cahn-Hilliard equation with a modified double-well potential $\tilde{f}(\phi)$ and the Allen-Cahn equation with a modified \tilde{g} . In the following, we drop the tilde $\tilde{\bullet}$ and assume both f and g satisfy conditions (i) and (ii) listed above.

We now present the numerical scheme as follows.

Semi-discrete scheme

Given the initial conditions $\mathbf{d}^0, \phi^0, \mathbf{u}^0$ and $p^0 = 0$, and having computed $\mathbf{d}^n, \phi^n, \mathbf{u}^n$ and p^n for $n \geq 0$, we compute $(\mathbf{d}^{n+1}, \phi^{n+1}, \mathbf{u}^{n+1}, p^{n+1})$ in the following sequence.

(1) Step 1: update \mathbf{d}^{n+1} :

$$\begin{cases} \frac{\mathbf{d}^{n+1} - \mathbf{d}^n}{\delta t} + \mathbf{u}_*^n \cdot \nabla \mathbf{d}^n - \mathbf{W}_*^n \cdot \mathbf{d}^n - a \mathbf{D}_*^n \cdot \mathbf{d}^n = M_1 \mathbf{h}^{n+1}, \\ \mathbf{h}^{n+1} = -C_1^n (\mathbf{d}^{n+1} - \mathbf{d}^n) + \nabla \cdot \left(\frac{K}{2} (\phi^n)^2 \nabla \mathbf{d}^{n+1} \right) - \frac{K}{2} (\phi^n)^2 g'(\mathbf{d}^n) \\ \quad - (A_1 - A_2) (\mathbf{d}^n \cdot \nabla \phi^n) \nabla \phi^n - A_2 |\nabla \phi^n|^2 \mathbf{d}^{n+1}, \\ \frac{\partial \mathbf{d}}{\partial \mathbf{n}} |_{\partial \Omega} = 0, \end{cases} \tag{3.3}$$

with $\mathbf{W}_*^n = \frac{1}{2} (\nabla \mathbf{u}_*^n - (\nabla \mathbf{u}_*^n)^T)$, $\mathbf{D}_*^n = \frac{1}{2} (\nabla \mathbf{u}_*^n + (\nabla \mathbf{u}_*^n)^T)$ and

$$\mathbf{u}_*^n = \mathbf{u}^n - \delta t \mathbf{h}^{n+1} \nabla \mathbf{d}^n + \delta t \nabla \cdot \left(\frac{1-a}{2} \mathbf{d}^n \mathbf{h}^{n+1} - \frac{1+a}{2} \mathbf{h}^{n+1} \mathbf{d}^n \right). \tag{3.4}$$

We impose an additional boundary condition $\mathbf{u}_*^n|_{\partial\Omega} = \mathbf{0}$ in this step when physical boundary conditions are imposed instead of the periodic boundary condition. This condition sometimes is satisfied automatically if the liquid crystal phase (denoted by $\phi = 1$) is completely inside Ω , namely, $\phi|_{\partial\Omega} = 0$ and $\nabla\phi|_{\partial\Omega} = \mathbf{0}$. By definition, $\mathbf{h}^{n+1}|_{\partial\Omega} = \mathbf{0}$ and $\mathbf{u}_*^n|_{\partial\Omega} = \mathbf{u}^n|_{\partial\Omega} = \mathbf{0}$. Otherwise, this new boundary condition serves as a bona fide intermediate boundary condition for \mathbf{d}^{n+1} .

(2) Step 2: update ϕ^{n+1} :

$$\begin{cases} \frac{\phi^{n+1} - \phi^n}{\delta t} + \nabla \cdot (\mathbf{u}_{**}^n \phi^n) = M_2 \Delta \mu^{n+1}, \\ \mu^{n+1} = C_2^n (\phi^{n+1} - \phi^n) + C_3^n (\Delta \phi^{n+1} - \Delta \phi^n) + \gamma (-\Delta \phi^{n+1} + f'(\phi^n)) \\ \quad + \phi^{n+1} W(\mathbf{d}^{n+1}) - (A_1 - A_2) \nabla \cdot ((\mathbf{d}^n \cdot \nabla \phi^n) \mathbf{d}^{n+1}) - A_2 \nabla \cdot (|\mathbf{d}^{n+1}|^2 \nabla \phi^{n+1}), \\ \frac{\partial \phi^{n+1}}{\partial \mathbf{n}}|_{\partial\Omega} = 0, \quad \frac{\partial \mu^{n+1}}{\partial \mathbf{n}}|_{\partial\Omega} = 0, \end{cases} \quad (3.5)$$

with $W(\mathbf{d}^{n+1}) = K \left(\frac{1}{2} |\nabla \mathbf{d}^{n+1}|^2 + g(\mathbf{d}^{n+1}) \right)$ and

$$\mathbf{u}_{**}^n = \mathbf{u}_*^n - \delta t \phi^n \nabla \mu^{n+1}. \quad (3.6)$$

(3) Step 3: update \mathbf{u}^{n+1} :

$$\begin{cases} \frac{\tilde{\mathbf{u}}^{n+1} - \mathbf{u}^n}{\delta t} + (\mathbf{u}^n \cdot \nabla) \tilde{\mathbf{u}}^{n+1} = \eta \Delta \tilde{\mathbf{u}}^{n+1} - \nabla p^n - \phi^n \nabla \mu^{n+1} \\ \quad - \mathbf{h}^{n+1} \nabla \mathbf{d}^n + \nabla \cdot \left(-\frac{a}{2} (\mathbf{d}^n \mathbf{h}^{n+1} + \mathbf{h}^{n+1} \mathbf{d}^n) + \frac{1}{2} (\mathbf{d}^n \mathbf{h}^{n+1} - \mathbf{h}^{n+1} \mathbf{d}^n) \right), \\ \tilde{\mathbf{u}}^{n+1}|_{\partial\Omega} = \mathbf{0}. \end{cases} \quad (3.7)$$

$$\begin{cases} \frac{\mathbf{u}^{n+1} - \tilde{\mathbf{u}}^{n+1}}{\delta t} = -\nabla(p^{n+1} - p^n), \\ \nabla \cdot \mathbf{u}^{n+1} = 0, \quad \mathbf{u}^{n+1} \cdot \mathbf{n}|_{\partial\Omega} = 0. \end{cases} \quad (3.8)$$

In the above, C_1^n , C_2^n and C_3^n are stabilizing parameters to be determined. The above scheme is constructed by combining several effective approaches in the approximation of Cahn–Hilliard equation [26], Navier–Stokes equations [10] and phase-field models [1,24].

Remark 3.1. A pressure-correction scheme [10] is used to decouple the computation of the pressure from that of the velocity.

Remark 3.2. We note that the explicit discretization of $f'(\phi) = \frac{2}{\varepsilon^2} \phi(1 - \phi)(1 - 2\phi)$ often leads to a severe restriction on time step δt when $\varepsilon \ll 1$. Thus, we introduce a “stabilizing” term to improve stability while preserving simplicity in (3.5), which allows us to treat the nonlinear term explicitly without subject to any time step constraint [26]. This stabilizing term introduces an error of order $O(\delta t)$ in a small region near the interface, the same order as the error introduced by treating $f(\phi)$ explicitly; so the overall truncation error of the scheme is essentially the same with or without the stabilizing term. A similar approach is applied to the director equation for the treatment of $g(\mathbf{d})$.

Remark 3.3. The scheme given by (3.3)–(3.8) is a fully decoupled, linear scheme. Hence, one only needs to solve a series of elliptic equations, which can be done very efficiently using fast solvers. Of course, some of these elliptic equations may be of variable coefficients.

Remark 3.4. If we don't study the embedded phase and boundary interaction when the boundary is primarily adjacent to the other phase, the new intermediate boundary condition on \mathbf{d}^{n+1} in practice can be avoided so long as we don't allow the embedded phase (for example, denoted by $\phi = 1$) to touch the boundary. This boundary condition is unnecessary if we deal with a periodic boundary condition.

We shall show next that the above scheme is energy stable unconditionally assuming each step can be solved uniquely.

4. Semi-discrete energy dissipation law

In this section, we prove that the scheme derived in the previous section is unconditionally energy stable. Instead of going directly to the proof, we first provide some lemmas to help readers to better follow the detail of the proof.

Lemma 4.1. Denote $\delta\phi^{n+1} = \phi^{n+1} - \phi^n$ and $\delta\delta\phi^{n+1} = \phi^{n+1} - 2\phi^n + \phi^{n-1}$. Then, the following equalities hold,

$$\begin{aligned} 2(\phi^{n+1} - \phi^n)\phi^{n+1} &= |\phi^{n+1}|^2 - |\phi^n|^2 + |\phi^{n+1} - \phi^n|^2, \\ 2(\phi^{n+1} - \phi^n)\phi^n &= |\phi^{n+1}|^2 - |\phi^n|^2 - |\phi^{n+1} - \phi^n|^2, \end{aligned}$$

$$\begin{aligned}
 &2(\nabla\phi^{n+1} - \nabla\phi^n) \cdot \nabla\phi^{n+1} + |\nabla\phi^{n+1}|^2 - |\nabla\phi^n|^2 + |\nabla\phi^{n+1} - \nabla\phi^n|^2, \\
 &2(\nabla\phi^{n+1} - \nabla\phi^n) \cdot \nabla\phi^n = |\nabla\phi^{n+1}|^2 - |\nabla\phi^n|^2 - |\nabla\phi^{n+1} - \nabla\phi^n|^2.
 \end{aligned}
 \tag{4.1}$$

Proof. We can obtain the equalities by simply expanding the inner product on the right hand side and then combining the common terms. \square

Lemma 4.2. If $F \in C^2(\mathbb{R}^k)$, where k is the dimension of the space, and

$$\max_{\mathbf{x} \in \mathbb{R}^k} |\mathbf{H}(\mathbf{x})| < L,
 \tag{4.2}$$

where \mathbf{H} is the Hessian matrix of F , $\forall \mathbf{x}^{n+1}, \mathbf{x}^n \in \mathbb{R}^k$, the following inequality holds,

$$(\mathbf{x}^{n+1} - \mathbf{x}^n) \cdot \nabla F(\mathbf{x}^n) \geq F(\mathbf{x}^{n+1}) - F(\mathbf{x}^n) - L|\mathbf{x}^{n+1} - \mathbf{x}^n|^2.
 \tag{4.3}$$

Proof. Notice the fact,

$$\begin{aligned}
 F(\mathbf{x}^{n+1}) &= F(\mathbf{x}^n) + \nabla F(\mathbf{x}^n) \cdot (\mathbf{x}^{n+1} - \mathbf{x}^n) + \int_{\mathbf{x}^n}^{\mathbf{x}^{n+1}} (\mathbf{x}^{n+1} - \mathbf{x}^n)^T \mathbf{H}(\mathbf{x}) \cdot d\mathbf{x} \\
 &\geq F(\mathbf{x}^n) + \nabla F(\mathbf{x}^n) \cdot (\mathbf{x}^{n+1} - \mathbf{x}^n) - L|\mathbf{x}^{n+1} - \mathbf{x}^n|^2.
 \end{aligned}
 \tag{4.4}$$

Then, we obtain

$$(\mathbf{x}^{n+1} - \mathbf{x}^n) \cdot \nabla F(\mathbf{x}^n) \geq F(\mathbf{x}^{n+1}) - F(\mathbf{x}^n) - L|\mathbf{x}^{n+1} - \mathbf{x}^n|^2. \quad \square
 \tag{4.5}$$

Lemma 4.3. The following identity holds,

$$\int_{\Omega} (\mathbf{v} \cdot \nabla) \mathbf{u} \cdot \mathbf{u} d\mathbf{x} = 0,
 \tag{4.6}$$

provided that $\mathbf{n} \cdot \mathbf{v}|_{\partial\Omega} = 0$, \mathbf{v} and \mathbf{u} are sufficiently smooth and $\nabla \cdot \mathbf{v} = 0$, where \mathbf{n} is the unit external normal of the surface $\partial\Omega$.

Proof. It is straightforward to show the following:

$$\begin{aligned}
 \int_{\Omega} (\mathbf{v} \cdot \nabla) \mathbf{u} \cdot \mathbf{u} d\mathbf{x} &= \int_{\Omega} \nabla \cdot \left(\mathbf{v} \frac{|\mathbf{u}|^2}{2} \right) - \frac{|\mathbf{u}|^2}{2} \nabla \cdot \mathbf{v} d\mathbf{x} \\
 &= \int_{\partial\Omega} \mathbf{n} \cdot \mathbf{v} \frac{|\mathbf{u}|^2}{2} ds \\
 &= 0. \quad \square
 \end{aligned}
 \tag{4.7}$$

Lemma 4.4. If C_1^n, C_2^n and C_3^n satisfy the following conditions,

$$\begin{aligned}
 C_1^n &\geq \frac{KL_2}{2} \|\phi^n\|_{\infty}^2 + \frac{1}{2} \max(A_1 - 2A_2, 0) \|\nabla\phi^n\|_{\infty}, \\
 C_2^n &\geq \gamma L_1, \\
 C_3^n &\geq \frac{1}{2} \max(A_1 - 2A_2, 0) \|\mathbf{d}^{n+1}\|_{\infty} - \frac{\gamma}{2},
 \end{aligned}
 \tag{4.8}$$

then

$$(\phi^{n+1} - \phi^n, \mu^{n+1}) - (\mathbf{d}^{n+1} - \mathbf{d}^n, \mathbf{h}^{n+1}) \geq F^{n+1} - F^n,
 \tag{4.9}$$

where F^n is the semi-discrete free energy defined as

$$\begin{aligned}
 F^n &= F_b^n + F_{\mathbf{d}}^n + F_{\text{anch}}^n, \\
 F_b^n &= \gamma \left(\frac{1}{2} |\nabla\phi^n|^2 + f(\phi^n), 1 \right), \\
 F_{\mathbf{d}}^n &= \left(\frac{1}{2} (\phi^n)^2 W(\mathbf{d}^n), 1 \right), \quad W(\mathbf{d}^n) = K \left(\frac{1}{2} |\nabla\mathbf{d}^n|^2 + g(\mathbf{d}^n) \right), \\
 F_{\text{anch}}^n &= \frac{A_1}{2} \left((\nabla\phi^n \cdot \mathbf{d}^n)^2, 1 \right) + \frac{A_2}{2} \left(|\mathbf{d}^n|^2 |\nabla\phi^n|^2 - (\nabla\phi^n \cdot \mathbf{d}^n)^2, 1 \right).
 \end{aligned}
 \tag{4.10}$$

Proof. Using the definition of μ^{n+1} in (3.5) and \mathbf{h}^{n+1} in (3.3), the first term on the left hand in (4.9) can be expanded as

$$\begin{aligned}
 (\phi^{n+1} - \phi^n, \mu^{n+1}) &= C_2^n \|\phi^{n+1} - \phi^n\|^2 + C_3^n \|\nabla\phi^{n+1} - \nabla\phi^n\|^2 \\
 &+ \frac{\gamma}{2} (\|\nabla\phi^{n+1}\|^2 - \|\nabla\phi^n\|^2 + \|\nabla\phi^{n+1} - \nabla\phi^n\|^2) + \gamma(\phi^{n+1} - \phi^n, f'(\phi^n)) \\
 &+ (\phi^{n+1} - \phi^n, \phi^{n+1}W(\mathbf{d}^{n+1})) - (\phi^{n+1} - \phi^n, (A_1 - A_2)\nabla \cdot ((\mathbf{d}^n \cdot \nabla\phi^n)\mathbf{d}^{n+1})) \\
 &+ (\phi^{n+1} - \phi^n, A_2\nabla \cdot (|\mathbf{d}^{n+1}|^2\nabla\phi^{n+1})).
 \end{aligned} \tag{4.11}$$

The second term on the left hand in (4.9) can be rewritten into the following

$$\begin{aligned}
 -(\mathbf{d}^{n+1} - \mathbf{d}^n, \mathbf{h}^{n+1}) &= C_1^n \|\mathbf{d}^{n+1} - \mathbf{d}^n\|^2 - (\mathbf{d}^{n+1} - \mathbf{d}^n, \nabla \cdot (\frac{K}{2}(\phi^n)^2\nabla\mathbf{d}^{n+1})) \\
 &+ (\mathbf{d}^{n+1} - \mathbf{d}^n, \frac{K}{2}(\phi^n)^2g'(\mathbf{d}^n)) + (A_1 - A_2)(\mathbf{d}^{n+1} - \mathbf{d}^n, (\mathbf{d}^n \cdot \nabla\phi^n)\nabla\phi^n) \\
 &+ A_2(\mathbf{d}^{n+1} - \mathbf{d}^n, |\nabla\phi^n|^2\mathbf{d}^{n+1}).
 \end{aligned} \tag{4.12}$$

We denote

$$\begin{aligned}
 T &= (\phi^{n+1} - \phi^n, \mu^{n+1}), \\
 T_0 &= C_2^n \|\phi^{n+1} - \phi^n\|^2 + C_3^n \|\nabla\phi^{n+1} - \nabla\phi^n\|^2, \\
 T_1 &= \gamma(\phi^{n+1} - \phi^n, f'(\phi^n)) + \frac{\gamma}{2} (\|\nabla\phi^{n+1}\|^2 - \|\nabla\phi^n\|^2 + \|\nabla\phi^{n+1} - \nabla\phi^n\|^2), \\
 T_2 &= (\phi^{n+1} - \phi^n, \phi^{n+1}W(\mathbf{d}^{n+1})), \\
 T_3 &= -(A_1 - A_2)(\phi^{n+1} - \phi^n, \nabla \cdot ((\mathbf{d}^n \cdot \nabla\phi^n)\mathbf{d}^{n+1})), \\
 T_4 &= -A_2(\phi^{n+1} - \phi^n, \nabla \cdot (|\mathbf{d}^{n+1}|^2\nabla\phi^{n+1})).
 \end{aligned} \tag{4.13}$$

In addition, we introduce

$$\begin{aligned}
 P &= -(\mathbf{d}^{n+1} - \mathbf{d}^n, \mathbf{h}^{n+1}), \\
 P_0 &= C_1^n \|\mathbf{d}^{n+1} - \mathbf{d}^n\|^2, \\
 P_1 &= -(\mathbf{d}^{n+1} - \mathbf{d}^n, \nabla \cdot (\frac{K}{2}(\phi^n)^2\nabla\mathbf{d}^{n+1})), \\
 P_2 &= (\mathbf{d}^{n+1} - \mathbf{d}^n, \frac{K}{2}(\phi^n)^2g'(\mathbf{d}^n)), \\
 P_3 &= (A_1 - A_2)(\mathbf{d}^{n+1} - \mathbf{d}^n, (\mathbf{d}^n \cdot \nabla\phi^n)\nabla\phi^n), \\
 P_4 &= A_2(\mathbf{d}^{n+1} - \mathbf{d}^n, |\nabla\phi^n|^2\mathbf{d}^{n+1}),
 \end{aligned} \tag{4.14}$$

such that

$$T = \sum_{i=0}^4 T_i, \quad P = \sum_{i=0}^4 P_i. \tag{4.15}$$

Next, we analyze these terms one-by-one. For T_1 , we have,

$$\begin{aligned}
 T_1 &= \gamma(\phi^{n+1} - \phi^n, f'(\phi^n)) + \frac{\gamma}{2} (\|\nabla\phi^{n+1}\|^2 - \|\nabla\phi^n\|^2 + \|\nabla\phi^{n+1} - \nabla\phi^n\|^2) \\
 &= \gamma(f(\phi^{n+1}) - f(\phi^n), 1) - \gamma L_1 \|\phi^{n+1} - \phi^n\|^2 + \frac{\gamma}{2} (\|\nabla\phi^{n+1}\|^2 - \|\nabla\phi^n\|^2 + \|\nabla\phi^{n+1} - \nabla\phi^n\|^2),
 \end{aligned} \tag{4.16}$$

i.e.

$$T_1 \geq F_b^{n+1} - F_b^n + \frac{\gamma}{2} \|\nabla\phi^{n+1} - \nabla\phi^n\|^2 - \gamma L_1 \|\phi^{n+1} - \phi^n\|^2. \tag{4.17}$$

For T_2 , we have,

$$\begin{aligned} T_2 &= (\phi^{n+1} - \phi^n, \phi^{n+1} W(\mathbf{d}^{n+1})) \\ &= \left(\frac{1}{2}(\phi^{n+1})^2 - \frac{1}{2}(\phi^n)^2, W(\mathbf{d}^{n+1})\right) + \frac{1}{2}((\phi^{n+1} - \phi^n)^2, W(\mathbf{d}^{n+1})) \\ &\geq \left(\frac{1}{2}(\phi^{n+1})^2 - \frac{1}{2}(\phi^n)^2, W(\mathbf{d}^{n+1})\right), \end{aligned} \quad (4.18)$$

if $W(\mathbf{d}) \geq 0, \forall \mathbf{d} \in \mathbb{R}^3$, which is true in our case.

For P_1 , we have

$$\begin{aligned} P_1 &= (\nabla \mathbf{d}^{n+1} - \nabla \mathbf{d}^n, \frac{K}{2}(\phi^n)^2 \nabla \mathbf{d}^{n+1}) \\ &= \left(\frac{K}{2}(\phi^n)^2, \frac{1}{2}(\nabla \mathbf{d}^{n+1})^2 - \frac{1}{2}(\nabla \mathbf{d}^n)^2\right) + \left(\frac{K}{2}(\phi^n)^2, \frac{1}{2}(\nabla \mathbf{d}^{n+1} - \nabla \mathbf{d}^n)^2\right) \\ &\geq \left(\frac{K}{2}(\phi^n)^2, \frac{1}{2}(\nabla \mathbf{d}^{n+1})^2 - \frac{1}{2}(\nabla \mathbf{d}^n)^2\right). \end{aligned} \quad (4.19)$$

For P_2 , we use Lemma 4.2 and obtain

$$\begin{aligned} P_2 &\geq \left(\frac{K}{2}(\phi^n)^2, g(\mathbf{d}^{n+1}) - g(\mathbf{d}^n)\right) - \left(\frac{K}{2}(\phi^n)^2, L_2(\mathbf{d}^{n+1} - \mathbf{d}^n)^2\right) \\ &\geq \left(\frac{K}{2}(\phi^n)^2, g(\mathbf{d}^{n+1}) - g(\mathbf{d}^n)\right) - \frac{L_2 K}{2} \|(\phi^n)^2\|_\infty \|\mathbf{d}^{n+1} - \mathbf{d}^n\|^2. \end{aligned} \quad (4.20)$$

Combining T_2 , P_1 and P_2 , we obtain

$$T_2 + P_1 + P_2 \geq F_{\mathbf{d}}^{n+1} - F_{\mathbf{d}}^n - \frac{L_2 K}{2} \|(\phi^n)^2\|_\infty \|\mathbf{d}^{n+1} - \mathbf{d}^n\|^2. \quad (4.21)$$

Combining T_3 and P_3 , we have

$$\begin{aligned} T_3 + P_3 &= (A_1 - A_2) \left(\left(\mathbf{d}^{n+1} - \mathbf{d}^n, (\mathbf{d}^n \cdot \nabla \phi^n) \nabla \phi^n \right) - \left(\phi^{n+1} - \phi^n, \nabla \cdot \left((\mathbf{d}^n \cdot \nabla \phi^n) \mathbf{d}^{n+1} \right) \right) \right) \\ &= (A_1 - A_2) \left(\left(\mathbf{d}^{n+1} - \mathbf{d}^n, (\mathbf{d}^n \cdot \nabla \phi^n) \nabla \phi^n \right) + \left(\nabla \phi^{n+1} - \nabla \phi^n, (\mathbf{d}^n \cdot \nabla \phi^n) \mathbf{d}^{n+1} \right) \right) \\ &= (A_1 - A_2) \left((\mathbf{d}^n \cdot \nabla \phi^n, \mathbf{d}^{n+1} \cdot \nabla \phi^{n+1}) - (\mathbf{d}^n \cdot \nabla \phi^n, \mathbf{d}^n \cdot \nabla \phi^n) \right) \\ &= \frac{A_1 - A_2}{2} \left(\|\mathbf{d}^{n+1} \cdot \nabla \phi^{n+1}\|^2 - \|\mathbf{d}^n \cdot \nabla \phi^n\|^2 - \|\mathbf{d}^{n+1} \cdot \nabla \phi^{n+1} - \mathbf{d}^n \cdot \nabla \phi^n\|^2 \right). \end{aligned} \quad (4.22)$$

Adding T_4 with P_4 , we have

$$\begin{aligned} T_4 + P_4 &= A_2 \left((\nabla \phi^{n+1} - \nabla \phi^n, |\mathbf{d}^{n+1}|^2 \nabla \phi^{n+1}) + (\mathbf{d}^{n+1} - \mathbf{d}^n, |\nabla \phi^n|^2 \mathbf{d}^{n+1}) \right) \\ &= \frac{A_2}{2} \left((|\nabla \phi^{n+1}|^2 - |\nabla \phi^n|^2 + |\nabla \phi^{n+1} - \nabla \phi^n|^2, |\mathbf{d}^{n+1}|^2) + (|\mathbf{d}^{n+1}|^2 - |\mathbf{d}^n|^2 + |\mathbf{d}^{n+1} - \mathbf{d}^n|^2, |\nabla \phi^n|^2) \right) \\ &= \frac{A_2}{2} \left(|\mathbf{d}^{n+1}|^2 |\nabla \phi^{n+1}|^2 - |\mathbf{d}^n|^2 |\nabla \phi^n|^2, 1 \right) + \frac{A_2}{2} (|\nabla \phi^{n+1} - \nabla \phi^n|^2, |\mathbf{d}^{n+1}|^2) + \frac{A_2}{2} (|\mathbf{d}^{n+1} - \mathbf{d}^n|^2, |\nabla \phi^n|^2). \end{aligned} \quad (4.23)$$

Combining T_3 , T_4 , P_3 and P_4 , we have

$$\begin{aligned} T_3 + T_4 + P_3 + P_4 &= F_{anch}^{n+1} - F_{anch}^n - \frac{A_1 - A_2}{2} (\|\mathbf{d}^{n+1} \cdot \nabla \phi^{n+1} - \mathbf{d}^n \cdot \nabla \phi^n\|^2) \\ &\quad + \frac{A_2}{2} (|\nabla \phi^{n+1} - \nabla \phi^n|^2, |\mathbf{d}^{n+1}|^2) + \frac{A_2}{2} (|\mathbf{d}^{n+1} - \mathbf{d}^n|^2, |\nabla \phi^n|^2). \end{aligned} \quad (4.24)$$

Note that

$$\begin{aligned}
 & -\|\mathbf{d}^{n+1} \cdot \nabla \phi^{n+1} - \mathbf{d}^n \cdot \nabla \phi^n\|^2 \\
 &= -\|\mathbf{d}^{n+1} \cdot \nabla \phi^{n+1} - \mathbf{d}^{n+1} \cdot \nabla \phi^n + \mathbf{d}^{n+1} \cdot \nabla \phi^n - \mathbf{d}^n \cdot \nabla \phi^n\|^2 \\
 &\geq -\|\mathbf{d}^{n+1} \cdot (\nabla \phi^{n+1} - \nabla \phi^n)\|^2 - \|\nabla \phi^n \cdot (\mathbf{d}^{n+1} - \mathbf{d}^n)\|^2 \\
 &\geq -(|\mathbf{d}^{n+1}|^2, |\nabla \phi^{n+1} - \nabla \phi^n|^2) - (|\nabla \phi^n|^2, |\mathbf{d}^{n+1} - \mathbf{d}^n|^2).
 \end{aligned} \tag{4.25}$$

Then, we have

$$\begin{aligned}
 T_3 + T_4 + P_3 + P_4 &\geq F_{anch}^{n+1} - F_{anch}^n \\
 &\quad - \frac{1}{2} \max(A_1 - 2A_2, 0) \left(\|(\mathbf{d}^{n+1})^2\|_\infty \|\nabla \phi^{n+1} - \nabla \phi^n\|^2 + \|(\nabla \phi^n)^2\|_\infty \|\mathbf{d}^{n+1} - \mathbf{d}^n\|^2 \right).
 \end{aligned} \tag{4.26}$$

Adding up (4.17), (4.21), (4.26), T_0 and P_0 , we have

$$\begin{aligned}
 & (\phi^{n+1} - \phi^n, \mu^{n+1}) - (\mathbf{d}^{n+1} - \mathbf{d}^n, \mathbf{h}^{n+1}) \\
 &= \sum_{i=0}^4 T_i + \sum_{i=0}^4 P_i \\
 &\geq F^{n+1} - F^n + C_2^n \|\phi^{n+1} - \phi^n\|^2 + C_3^n \|\nabla \phi^{n+1} - \nabla \phi^n\|^2 + C_1^n \|\mathbf{d}^{n+1} - \mathbf{d}^n\|^2 \\
 &\quad + \frac{\gamma}{2} \|\nabla \phi^{n+1} - \nabla \phi^n\|^2 - \gamma L_1 \|\phi^{n+1} - \phi^n\|^2 - \frac{KL_2}{2} \|\phi^n\|_\infty^2 \|\mathbf{d}^{n+1} - \mathbf{d}^n\|^2 \\
 &\quad - \frac{1}{2} \max(A_1 - 2A_2, 0) \left(\|(\mathbf{d}^{n+1})^2\|_\infty \|\nabla \phi^{n+1} - \nabla \phi^n\|^2 + \|(\nabla \phi^n)^2\|_\infty \|\mathbf{d}^{n+1} - \mathbf{d}^n\|^2 \right) \\
 &= F^{n+1} - F^n + (C_1^n - \frac{KL_2}{2} \|\phi^n\|_\infty^2 - \frac{1}{2} \max(A_1 - 2A_2, 0) \|\nabla \phi^n\|_\infty) \|\mathbf{d}^{n+1} - \mathbf{d}^n\|^2 \\
 &\quad + (C_2^n - \gamma L_1) \|\nabla \phi^{n+1} - \nabla \phi^n\|^2 + (C_3^n + \frac{\gamma}{2} - \frac{1}{2} \max(A_1 - 2A_2, 0) \|\mathbf{d}^{n+1}\|_\infty) \|\nabla \phi^{n+1} - \nabla \phi^n\|^2.
 \end{aligned} \tag{4.27}$$

By the assumption, we have,

$$\begin{aligned}
 C_1^n &\geq \frac{KL_2}{2} \|\phi^n\|_\infty^2 + \frac{1}{2} \max(A_1 - 2A_2, 0) \|\nabla \phi^n\|_\infty, \\
 C_2^n &\geq \gamma L_1, \\
 C_3^n &\geq \frac{1}{2} \max(A_1 - 2A_2, 0) \|\mathbf{d}^{n+1}\|_\infty - \frac{\gamma}{2}.
 \end{aligned} \tag{4.28}$$

Finally, we arrive at

$$(\phi^{n+1} - \phi^n, \mu^{n+1}) - (\mathbf{d}^{n+1} - \mathbf{d}^n, \mathbf{h}^{n+1}) \geq F^{n+1} - F^n. \quad \square \tag{4.29}$$

Theorem 4.1. Under the conditions in Lemma 4.4, the scheme (3.3)–(3.8) admits a unique solution satisfying the following semi-discrete energy dissipation law:

$$\begin{aligned}
 & \frac{1}{2} \|\mathbf{u}^{n+1}\|^2 + F^{n+1} + \frac{\delta t^2}{2} \|\nabla p^{n+1}\|^2 + \delta t \left(\eta \|\nabla \tilde{\mathbf{u}}^{n+1}\|^2 + M_2 \|\nabla \mu^{n+1}\|^2 + M_1 \|\mathbf{h}^{n+1}\|^2 \right) \\
 & \leq \frac{1}{2} \|\mathbf{u}^n\|^2 + F^n + \frac{\delta t^2}{2} \|\nabla p^n\|^2,
 \end{aligned} \tag{4.30}$$

where the semi-discrete energy F^n is defined in (4.10).

Proof. From the definition of \mathbf{u}_*^n in equation (3.4) and \mathbf{u}_{**}^n in equation (3.6), we can rewrite the momentum equation as follows

$$\frac{\tilde{\mathbf{u}}^{n+1} - \mathbf{u}_{**}^n}{\delta t} + (\mathbf{u}^n \cdot \nabla) \tilde{\mathbf{u}}^{n+1} - \eta \nabla^2 \tilde{\mathbf{u}}^{n+1} + \nabla p^n = 0. \tag{4.31}$$

Taking the inner-product of (4.31) with $2\delta t \tilde{\mathbf{u}}^{n+1}$, we obtain,

$$\|\tilde{\mathbf{u}}^{n+1}\|^2 - \|\mathbf{u}_{**}^n\|^2 + \|\tilde{\mathbf{u}}^{n+1} - \mathbf{u}_{**}^n\|^2 + 2\eta \delta t \|\nabla \tilde{\mathbf{u}}^{n+1}\|^2 + 2\delta t (\nabla p^n, \tilde{\mathbf{u}}^{n+1}) = 0. \tag{4.32}$$

To deal with the pressure term, we take the inner product of (3.8) with $2\delta t^2 \nabla p^n$ to arrive at

$$\delta t^2 (\|\nabla p^{n+1}\|^2 - \|\nabla p^n\|^2 - \|\nabla p^{n+1} - \nabla p^n\|^2) - 2\delta t (\tilde{\mathbf{u}}^{n+1}, \nabla p^n) = 0. \quad (4.33)$$

Taking the inner product of (3.8) with $2\delta t \mathbf{u}^{n+1}$, we obtain

$$\|\mathbf{u}^{n+1}\|^2 - \|\tilde{\mathbf{u}}^{n+1}\|^2 + \|\mathbf{u}^{n+1} - \tilde{\mathbf{u}}^{n+1}\|^2 = 0. \quad (4.34)$$

It follows from (3.8) directly that

$$\delta t^2 \|\nabla p^{n+1} - \nabla p^n\|^2 - \|\tilde{\mathbf{u}}^{n+1} - \mathbf{u}^{n+1}\|^2 = 0. \quad (4.35)$$

Adding up (4.32)–(4.35), we obtain

$$\|\mathbf{u}^{n+1}\|^2 - \|\mathbf{u}_{**}^n\|^2 + \|\tilde{\mathbf{u}}^{n+1} - \mathbf{u}_{**}^n\|^2 + \delta t^2 (\|\nabla p^{n+1}\|^2 - \|\nabla p^n\|^2) + 2\eta \delta t \|\nabla \tilde{\mathbf{u}}^{n+1}\|^2 = 0. \quad (4.36)$$

If we take the inner product of (3.3) with $-2\delta t \mathbf{h}^{n+1}$, we get

$$2\delta t M_1 \|\mathbf{h}^{n+1}\|^2 - 2\delta t (\mathbf{h}^{n+1}, (\mathbf{u}_{**}^n \cdot \nabla) \mathbf{d}^n) - 2(\mathbf{d}^{n+1} - \mathbf{d}^n, \mathbf{h}^{n+1}) + 2\delta t (\mathbf{h}^{n+1}, (\mathbf{W}_{**}^n + a\mathbf{D}_{**}^n) \cdot \mathbf{d}^n) = 0. \quad (4.37)$$

Taking the inner product of (3.4) with $2\mathbf{u}_{**}^n$, we obtain

$$\|\mathbf{u}_{**}^n\|^2 - \|\mathbf{u}^n\|^2 + \|\mathbf{u}_{**}^n - \mathbf{u}^n\|^2 + 2\delta t (\mathbf{h}^{n+1} \nabla \mathbf{d}^n, \mathbf{u}_{**}^n) - 2\delta t \left(\nabla \cdot \left(\frac{1-a}{2} \mathbf{d}^n \mathbf{h}^{n+1} - \frac{1+a}{2} \mathbf{h}^{n+1} \mathbf{d}^n \right), \mathbf{u}_{**}^n \right) = 0. \quad (4.38)$$

Adding (4.37) with (4.38) and noticing the fact that

$$\left(\nabla \cdot \left(\frac{1-a}{2} \mathbf{d}^n \mathbf{h}^{n+1} - \frac{1+a}{2} \mathbf{h}^{n+1} \mathbf{d}^n \right), \mathbf{u}_{**}^n \right) = \left(\mathbf{h}^{n+1}, (\mathbf{W}_{**}^n + a\mathbf{D}_{**}^n) \cdot \mathbf{d}^n \right), \quad (4.39)$$

we arrive at

$$\|\mathbf{u}_{**}^n\|^2 - \|\mathbf{u}^n\|^2 + \|\mathbf{u}_{**}^n - \mathbf{u}^n\|^2 + 2\delta t M_1 \|\mathbf{h}^{n+1}\|^2 - 2(\mathbf{d}^{n+1} - \mathbf{d}^n, \mathbf{h}^{n+1}) = 0. \quad (4.40)$$

If we take the inner product of (3.5) with $2\delta t \mu^{n+1}$, we obtain

$$2(\phi^{n+1} - \phi^n, \mu^{n+1}) + 2\delta t (\nabla \cdot (\phi^n \mathbf{u}_{**}^n), \mu^{n+1}) + 2M_2 \delta t \|\nabla \mu^{n+1}\|^2 = 0. \quad (4.41)$$

Taking the inner product of (3.6) with $2\mathbf{u}_{**}^n$, we have

$$\|\mathbf{u}_{**}^n\|^2 - \|\mathbf{u}_{**}^n\|^2 + \|\mathbf{u}_{**}^n - \mathbf{u}_{**}^n\|^2 + 2\delta t (\mathbf{u}_{**}^n, \phi^n \nabla \mu^{n+1}) = 0. \quad (4.42)$$

Adding (4.41) with (4.42), we arrive at

$$\|\mathbf{u}_{**}^n\|^2 - \|\mathbf{u}_{**}^n\|^2 + \|\mathbf{u}_{**}^n - \mathbf{u}_{**}^n\|^2 + 2(\phi^{n+1} - \phi^n, \mu^{n+1}) + 2M_2 \delta t \|\nabla \mu^{n+1}\|^2 = 0. \quad (4.43)$$

Finally, adding up the equations (4.36), (4.40), (4.43) and dividing both side by 2, we obtain

$$\begin{aligned} & \frac{1}{2} \left(\|\mathbf{u}^{n+1}\|^2 - \|\mathbf{u}^n\|^2 + \|\tilde{\mathbf{u}}^{n+1} - \mathbf{u}_{**}^n\|^2 \right) + \frac{1}{2} \delta t^2 (\|\nabla p^{n+1}\|^2 - \|\nabla p^n\|^2) + \eta \delta t \|\nabla \tilde{\mathbf{u}}^{n+1}\|^2 \\ & + \delta t M_2 \|\nabla \mu^{n+1}\|^2 + \delta t M_1 \|\mathbf{h}^{n+1}\|^2 + (\phi^{n+1} - \phi^n, \mu^{n+1}) - (\mathbf{d}^{n+1} - \mathbf{d}^n, \mathbf{h}^{n+1}) = 0. \end{aligned} \quad (4.44)$$

According to Lemma 4.4

$$(\phi^{n+1} - \phi^n, \mu^{n+1}) - (\mathbf{d}^{n+1} - \mathbf{d}^n, \mathbf{h}^{n+1}) \geq F^{n+1} - F^n, \quad (4.45)$$

hence, we finally obtain

$$\begin{aligned} & \frac{1}{2} \|\mathbf{u}^{n+1}\|^2 + F^{n+1} + \frac{\delta t^2}{2} \|\nabla p^{n+1}\|^2 + \delta t \left(\eta \|\nabla \tilde{\mathbf{u}}^{n+1}\|^2 + M_2 \|\nabla \mu^{n+1}\|^2 + M_1 \|\mathbf{h}^{n+1}\|^2 \right) \\ & \leq \frac{1}{2} \|\mathbf{u}^n\|^2 + F^n + \frac{\delta t^2}{2} \|\nabla p^n\|^2. \quad \square \end{aligned} \quad (4.46)$$

Here are several remarks regarding the constraints for C_1^n , C_2^n and C_3^n in Lemma 4.4.

Remark 4.1. Without the anchoring energy, the conditions in Lemma 4.4 reduce to $C_1^n \geq \frac{KL_2}{2} \|\phi^n\|_\infty^2$ and $C_2^n \geq \gamma L_1$. When the anchoring condition is weak such that $\frac{\gamma}{2} > \frac{1}{2} \max(A_1 - 2A_2, 0) \|\mathbf{d}^{n+1}\|^2$, the stabilizer C_3^n is not necessary.

Remark 4.2. The constraint for C_2^n is due to the explicit treatment of $f'(\phi)$ in the scheme (3.5) for ϕ^{n+1} . This constraint can be removed if we adopt convex splitting strategy [31] for $f'(\phi)$ or allow nonlinear schemes, i.e. treating $f(\phi)$ implicitly.

Remark 4.3. Although C_3^n explicitly depends on d^{n+1} , C_3^n only exists in the scheme (3.5) when solving ϕ^{n+1} , while \mathbf{d}^{n+1} has already been obtained. In this sense, as long as the constraint for C_3^n is satisfied, this scheme is energy stable for any time step δt .

5. Decoupled energy stable scheme for a reduced model

In the flow regime where $\|\mathbf{W}\|$ and $\|\mathbf{D}\|$ are small, a reduced model is obtained as follows:

$$\begin{cases} \partial_t \mathbf{u} + \mathbf{u} \cdot \nabla \mathbf{u} = -\nabla p + \eta \Delta \mathbf{u} - \phi \nabla \mu - \mathbf{h} \nabla \mathbf{d}, \\ \nabla \cdot \mathbf{u} = 0, \\ \partial_t \mathbf{d} + \mathbf{u} \cdot \nabla \mathbf{d} = M_1 \mathbf{h}, \\ \partial_t \phi + \nabla \cdot (\mathbf{u} \phi) = M_2 \Delta \mu, \end{cases} \tag{5.1}$$

where the chemical potential μ and molecular field \mathbf{h} are given respectively by

$$\begin{aligned} \mu &= \gamma(\Delta \phi - f(\phi)) - K\phi W(\mathbf{d}) - (A_1 - A_2) \nabla \cdot ((\mathbf{d} \cdot \nabla \phi) \mathbf{d}) - A_2 \nabla \cdot (|\mathbf{d}|^2 \nabla \phi), \\ \mathbf{h} &= \nabla \cdot \left(\frac{K\phi^2}{2} \nabla \mathbf{d} \right) + \frac{K\phi^2}{2} g'(\mathbf{d}) - (A_1 - A_2) (\mathbf{d} \cdot \nabla \phi) \nabla \phi - A_2 |\nabla \phi|^2 \mathbf{d}. \end{aligned} \tag{5.2}$$

An energy dissipation law exists for this model. In [27], a slightly different model in which the phase transport equation is the Allen–Cahn instead of the Cahn–Hilliard equation was studied. A first order energy stable scheme was devised and proved. For this model (eq. (5.1)), we devise a decoupled scheme below following our approach alluded to earlier.

Semi-discrete scheme

Given the initial conditions $\mathbf{d}^0, \phi^0, \mathbf{u}^0$ and $p^0 = 0$ and having computed $\mathbf{d}^n, \phi^n, \mathbf{u}^n$ and p^n for $n \geq 0$, we compute $(\mathbf{d}^{n+1}, \phi^{n+1}, \mathbf{u}^{n+1}, p^{n+1})$ in the following sequence.

(1) Step 1: update \mathbf{d}^{n+1} :

$$\begin{cases} \dot{\mathbf{d}}^{n+1} = M_1 \mathbf{h}^{n+1}, \\ \dot{\mathbf{d}}^{n+1} = \frac{\mathbf{d}^{n+1} - \mathbf{d}^n}{\delta t} + \mathbf{u}_*^n \cdot \nabla \mathbf{d}^n, \\ \mathbf{h}^{n+1} = -C_1^n (\mathbf{d}^{n+1} - \mathbf{d}^n) + \nabla \cdot \left(\frac{K}{2} (\phi^n)^2 \nabla \mathbf{d}^{n+1} \right) - \frac{K}{2} (\phi^n)^2 g'(\mathbf{d}^n) \\ \quad - (A_1 - A_2) (\mathbf{d}^n \cdot \nabla \phi^n) \nabla \phi^n - A_2 |\nabla \phi^n|^2 \mathbf{d}^{n+1}, \\ \frac{\partial \mathbf{d}}{\partial \mathbf{n}} \Big|_{\partial \Omega} = 0, \end{cases} \tag{5.3}$$

with

$$\mathbf{u}_*^n = \mathbf{u}^n - \delta t \mathbf{h}^{n+1} \nabla \mathbf{d}^n. \tag{5.4}$$

(2) Step 2: update ϕ^{n+1} :

$$\begin{cases} \dot{\phi}^{n+1} = M_2 \Delta \mu^{n+1}, \\ \mu^{n+1} = C_2^n (\phi^{n+1} - \phi^n) + C_3^n (\Delta \phi^{n+1} - \Delta \phi^n) + \gamma (-\Delta \phi^{n+1} + f'(\phi^n)) \\ \quad + \phi^{n+1} W(\mathbf{d}^{n+1}) - (A_1 - A_2) \nabla \cdot ((\mathbf{d}^n \cdot \nabla \phi^n) \mathbf{d}^{n+1}) - A_2 \nabla \cdot (|\mathbf{d}^{n+1}|^2 \nabla \phi^{n+1}), \\ \frac{\partial \phi^{n+1}}{\partial \mathbf{n}} \Big|_{\partial \Omega} = 0, \quad \frac{\partial \mu^{n+1}}{\partial \mathbf{n}} \Big|_{\partial \Omega} = 0, \end{cases} \tag{5.5}$$

with

$$\begin{aligned} \dot{\phi}^{n+1} &= \frac{\phi^{n+1} - \phi^n}{\delta t} + \nabla \cdot (\mathbf{u}_{**}^n \phi^n), \\ \mathbf{u}_{**}^n &= \mathbf{u}_*^n - \delta t \phi^n \nabla \mu^{n+1}, \\ W(\mathbf{d}^{n+1}) &= K \left(\frac{1}{2} |\nabla \mathbf{d}^{n+1}|^2 + g(\mathbf{d}^{n+1}) \right). \end{aligned} \tag{5.6}$$

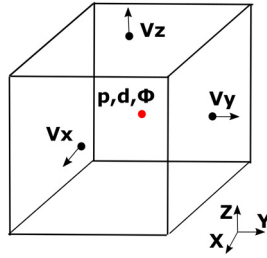


Fig. 6.1. Variable locations on the 3-D staggered grid.

(3) Step 3: update \mathbf{u}^{n+1} :

$$\begin{cases} \frac{\tilde{\mathbf{u}}^{n+1} - \mathbf{u}^n}{\delta t} + (\mathbf{u}^n \cdot \nabla) \tilde{\mathbf{u}}^{n+1} = \eta \Delta \tilde{\mathbf{u}}^{n+1} - \nabla p^n - \phi^n \nabla \mu^{n+1} - \mathbf{h}^{n+1} \nabla \mathbf{d}^n, \\ \tilde{\mathbf{u}}^{n+1}|_{\partial\Omega} = 0. \end{cases} \tag{5.7}$$

$$\begin{cases} \frac{\mathbf{u}^{n+1} - \tilde{\mathbf{u}}^{n+1}}{\delta t} = -\nabla(p^{n+1} - p^n), \\ \nabla \cdot \mathbf{u}^{n+1} = 0, \quad \mathbf{u}^{n+1} \cdot \mathbf{n}|_{\partial\Omega} = 0. \end{cases} \tag{5.8}$$

It can be proved analogously that the scheme is energy stable with respect to any δt . We omit the details since the proof is identical to the one we discussed previously in the paper. We comment on this reduced model because it has been a subject of intensive investigations by many numerical analysts and PDE analysts; physically it's applicability is limited, but it may be of mathematical and numerical values to some extent. In the next section, we will focus on the full model, its discretization and a couple of numerical results computed using it.

6. Numerical implementation and mesh refinement results

The first step (eq. (3.3)) in this semi-discrete, decoupled scheme is implicit. It involves a variable coefficient fourth order spatial operator with the coefficient proportional to δt . In order to solve this fourth order equation system, an additional boundary condition must be supplied as alluded to earlier. The solvability condition for this system is not yet established, not mention the uniqueness. However, if we drop the term proportional to δt in \mathbf{u}_*^n and use \mathbf{u}^n instead, the scheme remains first order in time and becomes a fully decoupled elliptic equation system. In the following, we will implement this simplified version of the scheme and study its behavior in mesh refinement. For simplicity in the implementation, we approximate \mathbf{u}_{**}^n by \mathbf{u}^n , which doesn't affect the order-of-accuracy of this scheme, i.e., it is still first-order accurate in time. Numerical tests show that energy decreases in time; so, the discrete energy dissipation law still holds numerically.

We denote the computational domain in space by $[0, L_x] \times [0, L_y] \times [0, L_z]$ where L_x, L_y, L_z are the length in x, y, z directions, respectively. In all the numerical studies presented below, we set

$$\delta t = 2 \times 10^{-4}, \quad \varepsilon = 0.01, \quad \delta = 0.03, \quad a = 1.2, \quad \gamma = 10, \tag{6.1}$$

where the choice of $a = 1.2$ indicate that the liquid crystal is rodlike. Then, we vary values of the other parameters in the various examples to be studied. We note a detailed parameter study is essential for investigating the physical properties of this LC model. However, in this paper, our goal is to illustrate the effectiveness of the proposed scheme instead of focusing on such a detailed parameter investigation.

6.1. Spatial discretization and GPU implementation

For the spatial operators in the scheme, we use second-order central finite difference methods to discretize them over a uniform spatial grid, where the velocity fields are discretized at the center of mesh surfaces, and pressure p , phase variables (ϕ and \mathbf{d}) are discretized at the cell center, as shown in Fig. 6.1. The boundary conditions are handled by ghost cells to maintain the spacial accuracy.

The fully discretized equations in the scheme are implemented on GPUs (graphics processing units) in 3 dimensional space and time for high-performance computing. To better utilize the performance of GPU, we store all variables in the global memory and store all parameters and mesh information (which do not change during the simulation) in the constant memory, which is the on-chip memory, such that it greatly reduces the latency of data access.

All the spatial discretizations are implemented the basic linear operators, such as the gradient, Laplacian, and divergence operator. For each time-step, we use a preconditioned Bi-Conjugate Gradient method to solve the linear equations, where the pre-conditioner is solved using FFT. For instance, in each time step, we need solving

$$L^n \psi^{n+1} = f^n, \tag{6.2}$$

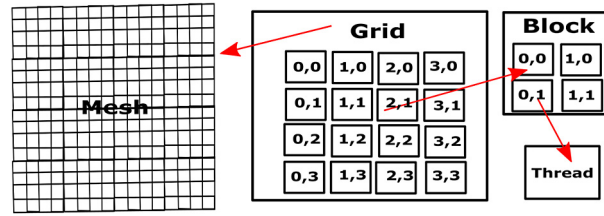


Fig. 6.2. 2D schematic of mapping from GPU threads to the mesh elements. This figure shows a 2D schematic on how each thread in a GPU implementation maps into a corresponding mesh element. Here, we have a 16×16 uniform mesh and claim 4×4 blocks in a grid, where each block contains 4 threads.

Table 6.1
CPU time vs. degrees of freedom.

Mesh	48^3	96^3	144^3	192^3	240^3
CPU time (seconds)	0.04	0.12	0.37	0.87	2.02

with ψ^{n+1} the variable, L^n a linear operator, f^n the right-hand-side, depending only on the variables in the n -th time step. We approximate L^n by a linear operator $\tilde{L}_n = \sum_{i=0}^k \lambda_i \Delta^i$, where $2k$ is less than or equal to the highest spatial derivative in L^n and λ_i are numerical weights. After having calculated \tilde{L}_n^{-1} by FFT, we solve

$$\tilde{L}_n^{-1} L^n \psi^{n+1} = \tilde{L}_n^{-1} f^n. \tag{6.3}$$

Instead of constructing the stiffness matrix (which takes memory storage on GPUs), we only need to apply linear operator $\tilde{L}_n^{-1} L^n$ on intermediate vectors (i.e. matrix vector multiplication), since we are using the Bi-Conjugate Gradient method, which is one of the Krylov subspace methods.

One advantage in using GPUs is its virtual allocations of processors (we can claim as many threads as we desire, even if it is beyond the existing number of multiprocessors on the physical device). Therefore, in our implementation, we allocate as many processors as the degree of freedom of the computed problem. A schematic is shown in Fig. 6.2, where we have a 16×16 uniform mesh, so we can claim 4×4 blocks with each block containing 4 threads. In this situation, there is a one to one mapping from the thread to the mesh point such that each thread calculates the respective component for the matrix vector multiplication. This strategy turns out to be very effective.

Remark 6.1. We note that the stability property of the full discretized scheme with the finite difference discretization in space is not yet established. Nor, are the corresponding fully discretized schemes with finite element, finite volume and spectral method, etc. Research in this direction still is ongoing.

6.2. Mesh refinement test

In order to have high resolution of spatial mesh size to eliminate the spatial error, here we test the code in 2D with the spatial mesh-size 512×512 and time step $\delta t = 2 \times 10^{-3}, 10^{-3}, 5 \times 10^{-4}, 2.5 \times 10^{-4}$ and 1.25×10^{-4} , respectively. At $t = 1$, the numerical solutions are compared. Here, we calculate the error by calculating the difference between the numerical result with the one of its nearest finer time step (which is regarded as the approximation to the accurate solution). The errors in L_1, L_2 and L_∞ norms are shown. The numerical tests demonstrate that the numerical scheme is at least first-order accurate in time. The mesh refinement test results are shown in Fig. 6.3.

In addition, we also summarize the CPU time for each time step versus varying mesh sizes (different nodes of freedom) in Table 6.1, where we choose $\delta t = 10^{-3}$. Our implementation is shown to be effective.

7. Numerical examples

7.1. Example 1: breakup of liquid crystal filaments

To demonstrate the power of this phase field model and the numerical code resulted from the new scheme we conduct a numerical simulation of the LC filament breakup phenomenon induced by capillary instability. The computational domain is chosen as $[0, 0.25] \times [0, 1] \times [0, 0.25]$ with $128 \times 512 \times 128$ grids. The initial orientation of the LCs parallels to the filament. We denote

$$r = \sqrt{(x - Lx/2)^2 + (z - Lz/2)^2}, \quad R = 0.03 + 0.005 \sin(2 \times \pi (y - Ly/2) + 0.5\pi). \tag{7.1}$$

The initial profile of the phase function ϕ is given by

$$\phi = \frac{1}{2} \left(\tanh\left(\frac{R-r}{\varepsilon}\right) + 1 \right). \tag{7.2}$$

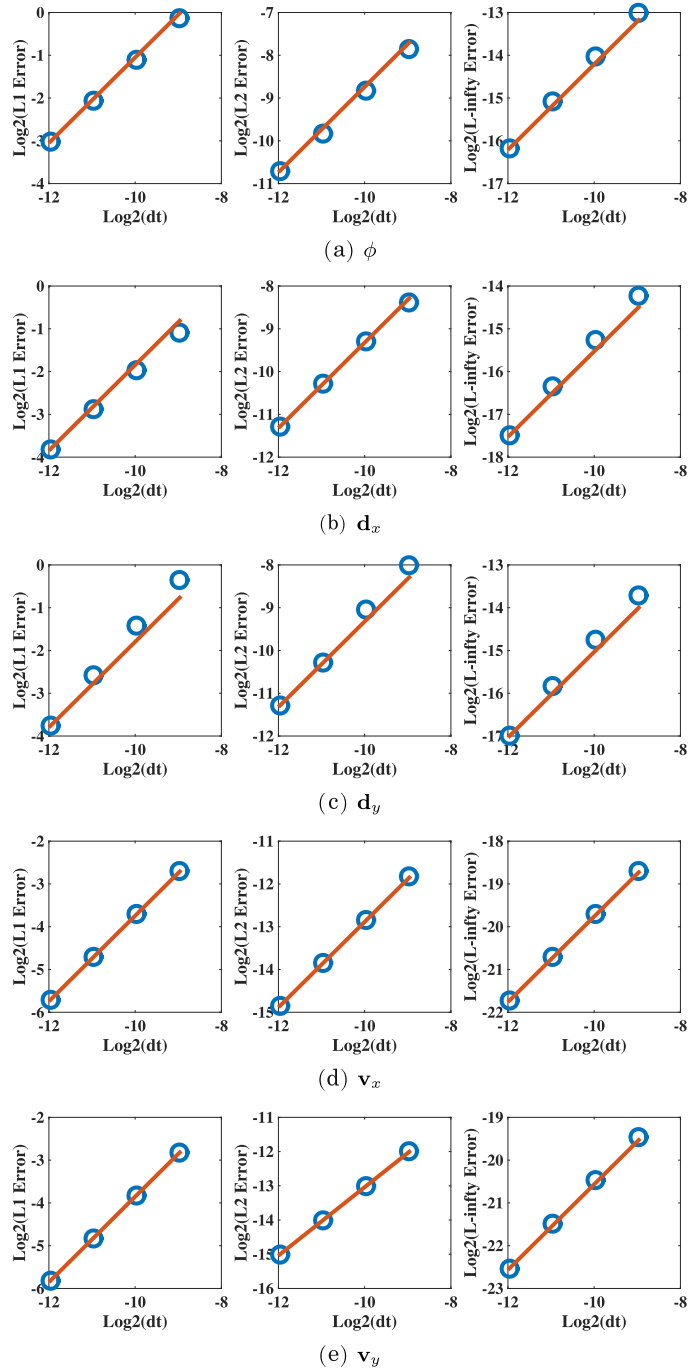


Fig. 6.3. Mesh refinement test in time. Here, we use spatial mesh size 512×512 , and choose time step $\delta t = 2 \times 10^{-3}$, 10^{-3} , 5×10^{-4} , 2.5×10^{-4} , 1.25×10^{-4} , respectively. The $\log_2(L_1, L_2, L_\infty$ norm of the error) for ϕ , \mathbf{v} and \mathbf{d} vs. $\log_2(\delta t)$ are plotted. The slope of the lines is 1.

The simulation result is shown in Fig. 7.1. In this computation, we do not impose any anchoring condition assuming the anchoring effect is weak. The filament eventually breaks up into satellite drops, where each drop shows a pair of defects located at the north and south pole, respectively. The bead on a string morphology is demonstrated, where we observe multiple small beads near a bigger one connected via thin liquid bridges. In order to observe the LC orientation and give a better view of interfacial dynamics, LC orientation is shown in Figs. 7.1(h)–(n), where 2D slices at $x = 0.5L_x$ are plotted. We observe that the LC aligns roughly in the direction of the axis of filament symmetry in the bulk; whereas at the LC-viscous fluid interface, the LC orientation is orthogonal to the normal of the interface at the interface leading to the pair of defects at the north and south pole. This phenomenon agrees qualitatively with the experimental finding.

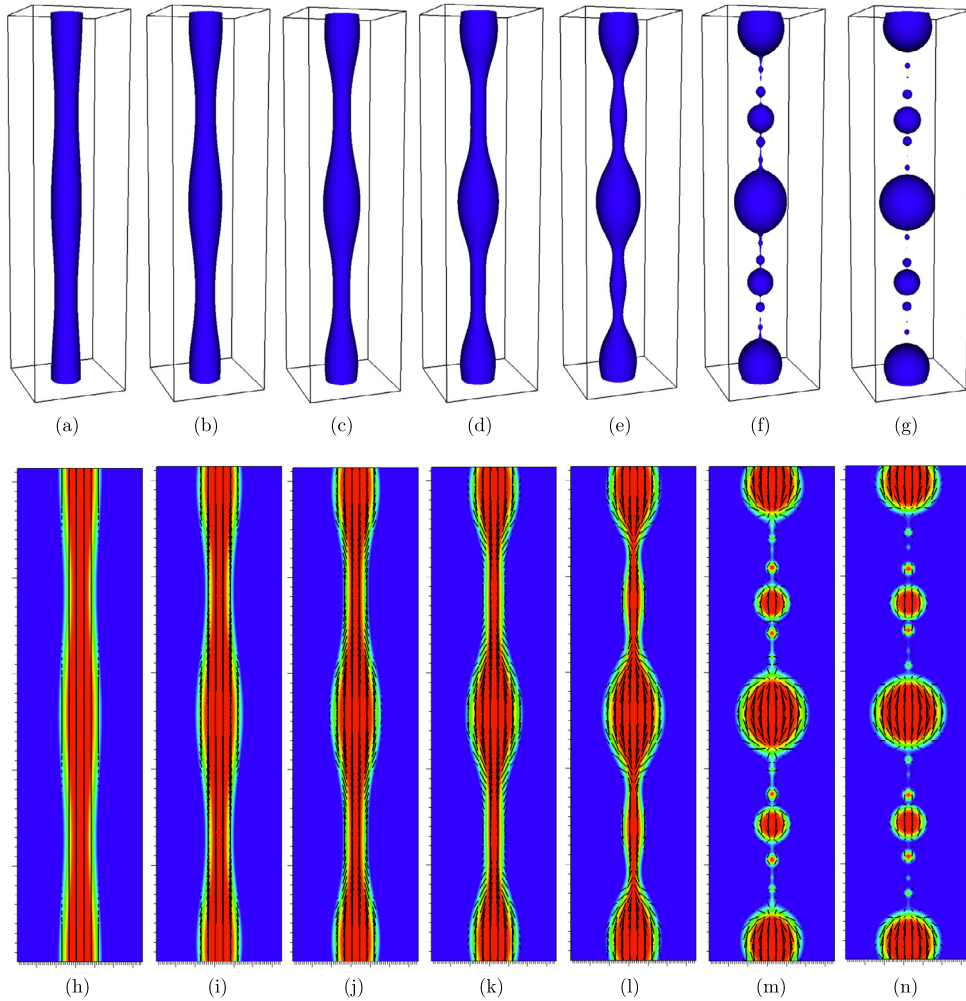


Fig. 7.1. Capillary instability of free liquid crystal jets. This figure shows beads formation induced by capillary instability with mesh $128 \times 512 \times 128$ and domain size $[0, 0.25] \times [0, 1] \times [0, 0.25]$. A time series ($t = 0, 1, 2, 3, 4, 5, 6$) of 3D view is shown in (a)–(g), respective 2D view is shown in (h)–(n). The parameters are $\delta t = 5.0 \times 10^{-4}$, $\eta = 1.0$, $M_1 = 1.0 \times 10^{-10}$, $M_2 = 1.0 \times 10^{-3}$, $K = 0.025$, $A_1 = A_2 = 0$.

7.2. Example 2: a liquid crystal drop in a shear flow of viscous fluids

In this example, we simulate the shear induced rupture of a liquid crystal drop. Initially, a spherical liquid crystal drop is placed in a viscous fluid matrix with the same density and viscosity. The parallel plates ($y = 0, Ly$) moves in the opposite direction with relative speed $v_0 = 20$. One numerical result is shown in Fig. 7.2 and Fig. 7.3. The drop first elongates due to the shearing flow. After it elongates into a filament, it ruptures into satellite drops or beads. We also conduct a comparative study on the rupture phenomenon of liquid crystal drops with respect to various Frank-elastic constant K and plot the results in Fig. 7.4, where we observe that a high Frank-elastic constant facilitates the rupture of the drop into more satellite drops than it is small.

8. Conclusion

In this paper, we present a hydrodynamic phase field model derived using the generalized Onsager principle, which obeys an energy dissipative law even with the anchoring condition incorporated. We then design a linear, first-order, decoupled, energy stable scheme for the full model and show that the semi-discrete scheme satisfies an analogous, discrete energy dissipation law. While we have only considered the semi-discrete scheme in time, the results can be carried over to the fully discrete scheme for any consistent finite element or spectral Galerkin approximations since the proof is based on the variational formulation with all test functions in the same space as the trial function. We further implement the scheme with a finite difference method in space on GPUs for high performance computing. Two 3D numerical examples are shown to illustrate the power of this code in resolving complex interfacial fluid dynamics. More detailed studies on dynamics of nematic liquid crystal drops will be given in a sequel.

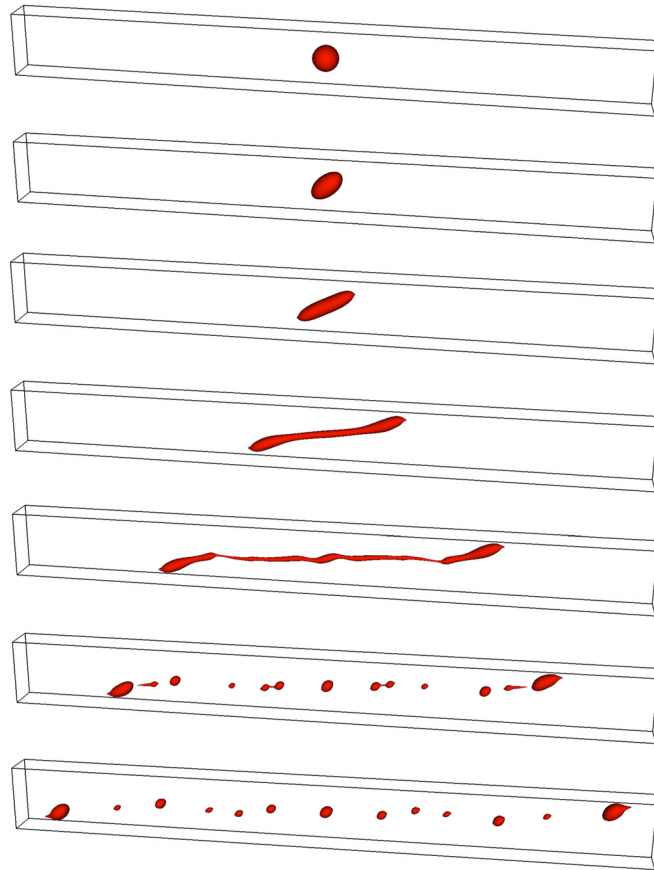


Fig. 7.2. 3D simulation of shear induced rupture of a liquid crystal drop in a viscous fluid. This figure shows a time sequence ($t = 0, 0.4, 0.8, 1.2, 1.6, 1.8, 2.0$) of a liquid crystal drop in a viscous shear flow field induced by a moving boundary. The moving speed, which is also the shear rate in this paper, is 20 in the simulation. The domain is $[0, 0.5] \times [0, 1] \times [0, 10]$ with mesh $64 \times 128 \times 1280$, $\delta t = 5.0 \times 10^{-4}$, $\eta = 0.1$, $M_1 = 2.5 \times 10^{-6}$, $M_2 = 1.0 \times 10^{-3}$, $K = 0.05$, $A_1 = A_2 = 0$.

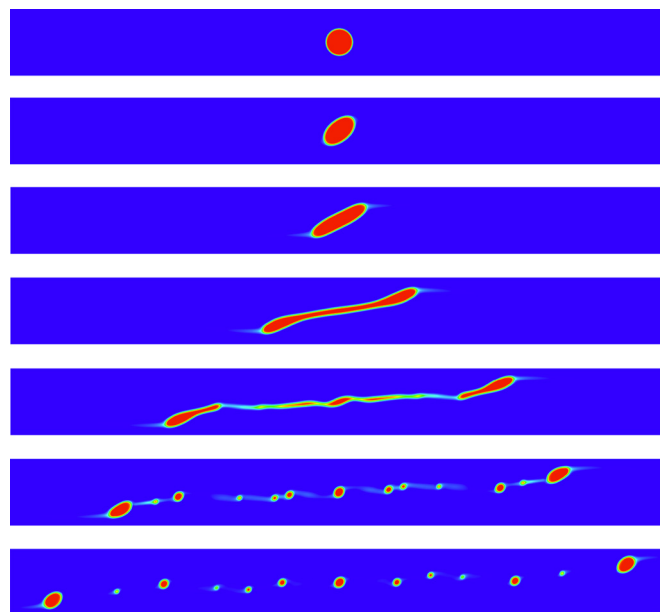


Fig. 7.3. 3D simulation of shear induced rupture of liquid crystal drop in a viscous fluid. This shows a 2D view of the dynamics shown in Fig. 7.2 at ($t = 0, 0.4, 0.8, 1.2, 1.6, 1.8, 2.0$).

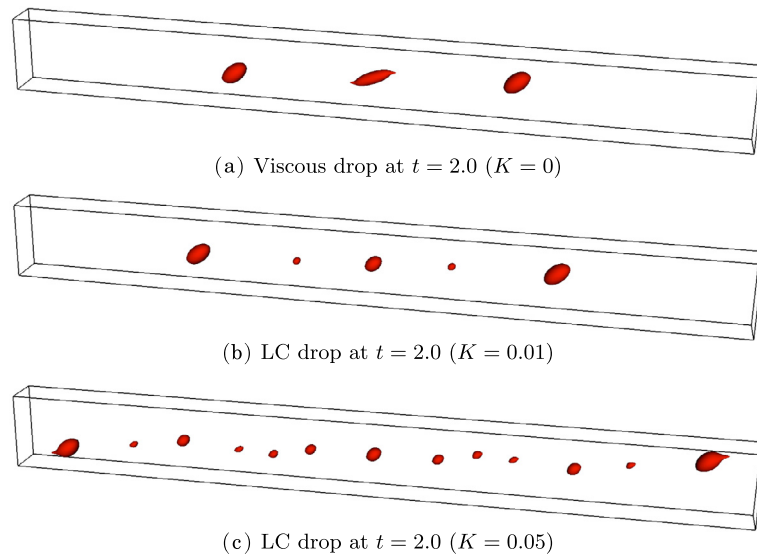


Fig. 7.4. The effect of distortional elasticity K on the shear induced rupture of the liquid crystal drop. These figures show that the micro-structure of the liquid crystal enhances the shear induced rupture in that the stronger the distortional elasticity of the liquid crystal is, the more satellite drops are produced by shear. All the other parameters are the same as in Fig. 7.2, except: (A) $K = 0$; (B) $K = 0.01$; (C) $K = 0.05$.

Acknowledgements

Jia Zhao and Qi Wang are partially supported by NSF-DMS-1200487, NSF-DMS-1517347, NIH-2R01GM078994-05A1, AFOSR-FA9550-12-1-0178, and an SC EPSCOR/IDEA award. J. Shen is partially supported by NSF-DMS-1215066 and AFOSR FA9550-11-1-0328. X. Yang is partially supported by NSF-DMS-1200487, AFOSR-FA9550-12-1-0178. In addition, Jia Zhao is also supported by a Dissertation Fellowship from the Provost Office of USC.

References

- [1] Franck Boyer, Sebastian Minjeaud, Numerical schemes for a three component Cahn–Hilliard model, *ESAIM: Math. Model. Numer. Anal.* 45 (4) (2011) 697–738.
- [2] J.W. Cahn, J.E. Hilliard, Free energy of a nonuniform system. I. Interfacial free energy, *J. Chem. Phys.* 28 (1958) 258–267.
- [3] L.Q. Chen, J. Shen, Applications of semi-implicit Fourier–spectral method to phase field equations, *Commun. Comput. Phys.* 108 (1998) 147–158.
- [4] L.Q. Chen, Y. Wang, The continuum field approach to modeling microstructural evolution, *JOM* 48 (1996) 13–18.
- [5] N. Condette, C. Melcher, E. Suli, Spectral approximation of pattern-forming nonlinear evolution equations with double-well potentials of quadratic growth, *Math. Comput.* 80 (2011) 205–223.
- [6] P.G. de Gennes, J. Prost, *The Physics of Liquid Crystals*, Oxford University Press, 1993.
- [7] Q. Du, M. Li, C. Liu, Analysis of a phase field Navier–Stokes vesicle–fluid interaction model, *Discrete Contin. Dyn. Syst., Ser. B* 8 (3) (2007) 539–556.
- [8] J.L. Ericksen, Conservation laws for liquid crystals, *Trans. Soc. Rheol.* 5 (1961) 23–34.
- [9] A. Fick, Poggendorff’s annalen, *J. Am. Math. Soc.* (1855) 59–86.
- [10] J.L. Guermond, P. Mineev, J. Shen, An overview of projection methods for incompressible flows, *Comput. Methods Appl. Mech. Eng.* 195 (2006) 6011–6045.
- [11] M.E. Gurtin, D. Polignone, J. Viñals, Two-phase binary fluids and immiscible fluids described by an order parameter, *Math. Models Methods Appl. Sci.* 6 (6) (1996) 815–831.
- [12] D. Jacqmin, Diffuse interface model for incompressible two-phase flows with large density ratios, *J. Comput. Phys.* 155 (1) (2007) 96–127.
- [13] B. Jerome, Surface effects and anchoring in liquid crystals, *Rep. Prog. Phys.* 54 (1991) 391.
- [14] Daniel Kessler, Ricardo H. Nochetto, Alfred Schmidt, A posteriori error control for the Allen–Cahn problem: circumventing Gronwall’s inequality, *M2AN Math. Model. Numer. Anal.* 38 (1) (2004) 129–142.
- [15] Junseok Kim, Phase-field models for multi-component fluid flows, *Commun. Comput. Phys.* 12 (3) (2012) 613–661.
- [16] F.M. Leslie, Some constitutive equations for anisotropic fluids, *Q. J. Mech. Appl. Math.* 19 (1966) 357–370.
- [17] F.M. Leslie, Some constitutive equations for liquid crystals, *Arch. Ration. Mech. Anal.* 28 (1968) 265–283.
- [18] F.H. Lin, On nematic liquid crystals with variable degree of orientation, *Commun. Pure Appl. Math.* 44 (1991) 453–468.
- [19] F.H. Lin, *Mathematics theory of liquid crystals*, in: *Applied Mathematics at the Turn of Century*, 1995.
- [20] C. Liu, J. Shen, X. Yang, Dynamics of defect motion in nematic liquid crystal flow: modeling and numerical simulation, *Commun. Comput. Phys.* 2 (6) (2007) 1184–1198.
- [21] C. Liu, N.J. Walkington, An Eulerian description of fluids containing visco-hyperelastic particles, *Arch. Ration. Mech. Anal.* 159 (2001) 229–252.
- [22] Chun Liu, Jie Shen, A phase field model for the mixture of two incompressible fluids and its approximation by a Fourier–spectral method, *Physica D* 179 (3–4) (2003) 211–228.
- [23] L. Rayleigh, On the theory of surface forces—II. Compressible fluids, *Philos. Mag.* 33 (1892).
- [24] J. Shen, X. Yang, A phase-field model and its numerical approximation for two-phase incompressible flows with different densities and viscosities, *SIAM J. Sci. Comput.* 32 (2010) 1159–1179.
- [25] Jie Shen, Modeling and numerical approximation of two-phase incompressible flows by a phase-field approach, in: *Multiscale Modeling and Analysis for Materials Simulation*, 2011, pp. 147–196.

- [26] Jie Shen, Xiaofeng Yang, Numerical approximation of Allen–Cahn and Cahn–Hilliard equations, *Discrete Contin. Dyn. Syst., Ser. B* 28 (4) (2010) 1669–1691.
- [27] Jie Shen, Xiaofeng Yang, Decoupled energy stable schemes for phase field models of two phase complex fluids, *SIAM J. Sci. Comput.* 36 (1) (2014) 122–145.
- [28] Jie Shen, Xiaofeng Yang, Qi Wang, Mass and volume conservation in phase field models for binary fluids, *Commun. Comput. Phys.* 13 (4) (2013) 1045–1065.
- [29] Pengtao Sun, Chun Liu, Jinchao Xu, Phase field model of thermo-induced Marangoni effects in the mixtures and its numerical simulations with mixed finite element methods, *Commun. Comput. Phys.* 6 (2009) 1095–1117.
- [30] J. van der Waals, The thermodynamic theory of capillarity under the hypothesis of a continuous density variation, *J. Stat. Phys.* 20 (1893) 197–244.
- [31] S.M. Wise, C. Wang, J.S. Lowengrub, An energy-stable and convergent finite-difference scheme for the phase field crystal equation, *SIAM J. Numer. Anal.* 47 (3) (2009) 2269–2288.
- [32] X. Yang, M.G. Forest, H. Li, C. Liu, J. Shen, Q. Wang, F. Chen, Modeling and simulations of drop pinch-off from liquid crystal filaments and the leaky liquid crystal faucet immersed in viscous fluids, *J. Comput. Phys.* 236 (2013) 1–14.
- [33] Xiaogang Yang, Qi Wang, Capillary instability of axisymmetric active liquid crystal jets, *Soft Matter* 10 (35) (2014) 6758–6776.
- [34] P. Yue, J.J. Feng, C. Liu, J. Shen, A diffuse-interface method for simulating two-phase flows of complex fluids, *J. Fluid Mech.* 515 (2004) 293–317.
- [35] Shupeng Zhang, Chun Liu, Hui Zhang, Numerical simulation of hydrodynamics of nematic liquid crystals: effects of kinematic transports, *Commun. Comput. Phys.* 9 (4) (2011) 974.
- [36] Tianyu Zhang, Nick G. Cogan, Qi Wang, Phase-field models for biofilms II. 2-D numerical simulations of biofilm–flow interaction, *Commun. Comput. Phys.* 4 (1) (2008) 72–101.
- [37] Jingzhi Zhu, Longqing Chen, Jie Shen, Veena Tikare, Coarsening kinetics from a variable-mobility Cahn–Hilliard equation: application of a semi-implicit Fourier spectral method, *Phys. Rev. E* 60 (1999) 3564.